Organic Frameworks

International Edition: DOI: 10.1002/anie.201700271
German Edition: DOI: 10.1002/ange.201700271

Twisted Aromatic Frameworks: Readily Exfoliable and Solution-Processable Two-Dimensional Conjugated Microporous Polymers

*A. Belen Marco, Diego Cortizo-Lacalle, Iñigo Perez-Miqueo, Giovanni Valenti, Alessandro Boni, Jan Plas, Karol Strutyński, Steven De Feyter, Francesco Paolucci, Mario Montes, Andrei N. Khlobystov, Manuel Melle-Franco, and Aurelio Mateo-Alonso**

Abstract: *Twisted two-dimensional aromatic frameworks have been prepared by overcrowding the nodes with bulky and rigid substituents. The highly distorted aromatic framework with alternating out-of-plane substituents results in diminished interlayer interactions that favor the exfoliation and dispersion of individual layers in organic media.*

The discovery of graphene[1] has opened up exciting possibilities for developing two-dimensional (2D) polymers,[2] such as 2D conjugated microporous polymers (2D-CMPs) and 2D covalent organic frameworks (2D-COFs), for a wide range of applications,[2] including electronics, energy conversion and storage, gas storage and separation, catalysis, and sensing. Synthetic 2D organic frameworks composed of fused aromatic rings[3] have emerged as a highly tunable alternative to nanopore-grafted (or holey) graphene, since they combine an extended 2D π system with permanent nanometer-sized pores. Furthermore, since such 2D polymers are synthesized by bottom-up approaches, heteroatoms can be incorporated into the framework with relative ease, which provides an additional way to modulate their electronic structure and their properties. For example, the exchange of C atoms for N atoms in 2D organic frameworks has resulted in more efficient materials for energy applications, such as electrocatalysts for the oxygen reduction reaction (ORR),[4] the hydrogen evolution reaction (HER),[5] supercapacitors,[6] and batteries.[6a,7]

The preparation of stable dispersions of individual layers of 2D organic frameworks would be ideal from several perspectives. First, it would facilitate the sorting of layers by size, composite preparation by solution mixing, chemical modification, and structural and optoelectronic characterization.[8] Second, it would enable the formulation of such 2D materials in inks[8] and thus would enable low-cost, large-area liquid-deposition methods, such as spin coating, spray coating, or inkjet printing. However, similarly to graphene, synthetic 2D organic frameworks are very difficult to process because of the great tendency of the individual layers to aggregate by noncovalent interlayer interactions. Although several examples of the delamination of 2D organic frameworks by mechanical[9] and solvent-assisted methods,[10] electrostatic repulsion,[11] and chemical methods[12] have been reported, these methods provide materials that are a few layers thick and thereby show that the individualization of layers is still a challenging task.

Herein, we report a new and unconventional approach for obtaining dispersions of individual layers of 2D-CMPs composed of fused aromatic rings on the basis of the introduction of twists in their framework by overcrowding the nodes of the framework with bulky and rigid substituents, which are forced above and below the plane (Figure 1). The highly distorted aromatic framework with alternating out-of-plane substituents results in diminished interlayer interactions, thus favoring the exfoliation and dispersion of individual layers in organic media and leading to stable dispersions that can be processed into thin films. Direct drop casting of a dispersion of the twisted 2D-CMP on glass and on glassy-

[*] Dr. A. B. Marco, Dr. D. Cortizo-Lacalle, Prof. Dr. A. Mateo-Alonso
POLYMAT, University of the Basque Country UPV/EHU
Avenida de Tolosa 72, 20018 Donostia-San Sebastian (Spain)
E-mail: amateo@polymat.eu
Homepage: http://www.polymat.eu
Prof. Dr. A. Mateo-Alonso
Ikerbasque, Basque Foundation for Science
48011 Bilbao (Spain)
I. Perez-Miqueo, Prof. Dr. M. Montes
Grupo de Ingeniería Química
Dto. de Química Aplicada Fac. de C. Químicas, UPV/EHU
Apdo 1072, 20080 San Sebastián (Spain)
Dr. G. Valenti, Dr. A. Boni, Prof. Dr. F. Paolucci
Dipartimento di Chimica "Giacomo Ciamician"
Via Selmi 2, 40126 Bologna (Italy)
Dr. J. Plas, Prof. Dr. S. De Feyter
KU Leuven, Department of Chemistry
Division of Molecular Imaging and Photonics
Celestijnenlaan 200F, 3001 Leuven (Belgium)
Prof. Dr. A. N. Khlobystov
School of Chemistry, University of Nottingham
University Park, Nottingham (UK)
Dr. K. Strutyński, Prof. Dr. M. Melle-Franco
CICECO—Aveiro Institute of Materials
Department of Chemistry, University of Aveiro
3810-193 Aveiro (Portugal)

Supporting information for this article can be found under: http://dx.doi.org/10.1002/anie.201700271.

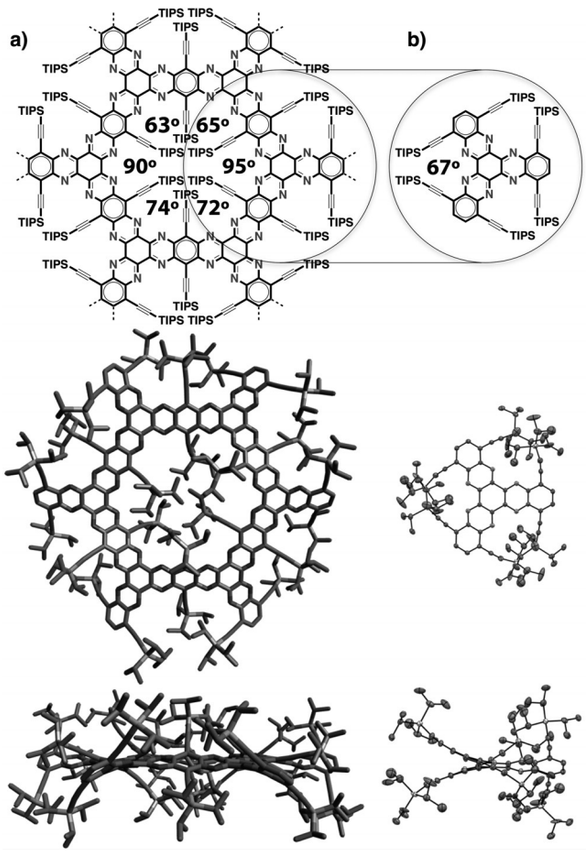

Figure 1. a) Chemical structure (with twist angles) of TIPS-CMP and PM6-DH2 calculated structure of a closed pore of TIPS-CMP (top and side views). b) Chemical structure (with twist angle) and crystal structure[13] of twisted-HATNA (top and side views). Hydrogen atoms have been omitted from all structures for clarity.

carbon electrodes showed the semiconducting nature and the ORR activity of this new member of the 2D materials family.

Our twisting approach for the preparation of a 2D-CMP is based on the introduction of rigid acetylene moieties with triisopropylsilyl (TIPS) groups at the nodes of the framework (Figure 1). In analogy to twisted 1,4,7,10,13,16-hexa(triisopropylsilyl)ethynyl-5,6,11,12,17,18-hexaazatrinaphthylene (twisted-HATNA),[13,14] the close proximity of the TIPS groups will force the aromatic framework to deviate from planarity, as there is not sufficient space to accommodate all the substituents in the same plane. We envisioned the preparation of a twisted 2D-CMP by using the conditions described for the synthesis of pyrazine-fused conjugated microporous polymers (Aza-CMPs)[3a] by Jiang and co-workers (Scheme 1). However, the Aza-CMPs were synthesized by ionothermal methods, which require harsh conditions incompatible with TIPS substituents. For this reason, we first established a solvothermal method to prepare Aza-CMPs under milder conditions, namely, the cyclocondensation of 1,2,4,5-benzenetetraamine and 1,2,3,4,5,6-hexaketocyclohexane in a 1:4 mixture of dioxane and acetic acid at reflux. These solvothermal conditions provided Aza-CMP with nearly

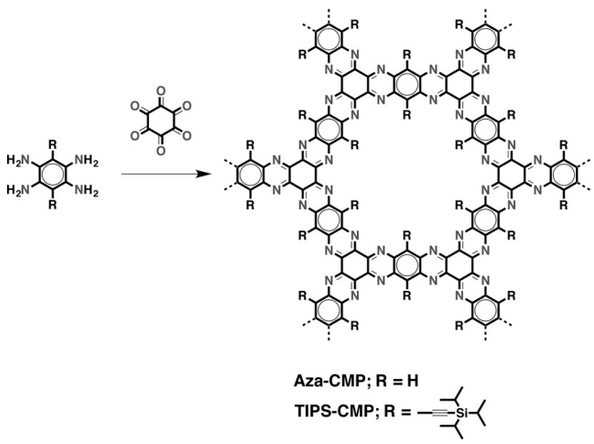

Scheme 1. Solvothermal synthesis and structures of Aza-CMP and TIPS-CMP.

identical structural data (see Figures S1, S2, S3, S4, and S7 in the Supporting Information) to those of Aza-CMPs obtained by ionothermal methods at low temperatures.[3a] The cyclocondensation of 1,2,3,4,5,6-hexaketocyclohexane with 3,6-di(triisopropylsilyl)ethynyl-1,2,4,5-benzenetetraamine[15] in a 1:4 mixture of dioxane and acetic acid at reflux yielded TIPS-CMP after purification (Scheme 1).

The structure of TIPS-CMP was confirmed by a combination of different characterization techniques (see the Supporting Information for details). In the FTIR spectrum of TIPS-CMP, the vibration bands corresponding to the monomers had disappeared, and new bands in agreement with those of Aza-CMP, which was used as a planar reference, were observed (Figure 2a; see also Figure S1). The FTIR spectrum of TIPS-CMP (Figure 2a) showed the disappearance of both the C=O (1663 cm^{-1}) and NH_2 (3444 and 3363 cm^{-1}) groups of the precursors. The formation of new C–N bonds was evidenced by the appearance of an intense band at 1202 cm^{-1} as a result of the C–C and C–N stretching of the pyrazine rings, and the shift in the typical features of the aromatic rings from the starting material (1540 and 1460 cm^{-1}) to TIPS-CMP (1515 and 1454 cm^{-1}). $C(sp^3)$–H stretching vibrations were present in the spectra of both the starting tetraamine and TIPS-CMP, and although a small feature at 2131 cm^{-1} could be observed for TIPS-CMP, the band corresponding to the C=N/C=C stretching mode had almost disappeared, as expected for highly symmetric structures. These changes in the spectra were also reproduced in the case of Aza-CMP, for which the bands at 2892 (N–H) and 1663 cm^{-1} (C=O) were not present in the final polymer, and an intense band at 1216 cm^{-1} indicative of the formation of the pyrazine rings was observed. Solid-state cross-polarization/magic-angle spinning (CP/MAS) NMR spectroscopy of TIPS-CMP was consistent with the proposed structure. The ^1H NMR spectrum of TIPS-CMP showed a signal centered at 0.12 ppm corresponding to the hydrogen atoms of the TIPS groups (Figure 2b). As expected, the ^{13}C NMR spectrum of TIPS-CMP showed a broad signal (typical of quaternary carbon atoms) corresponding to the sp^2- and sp-hybridized

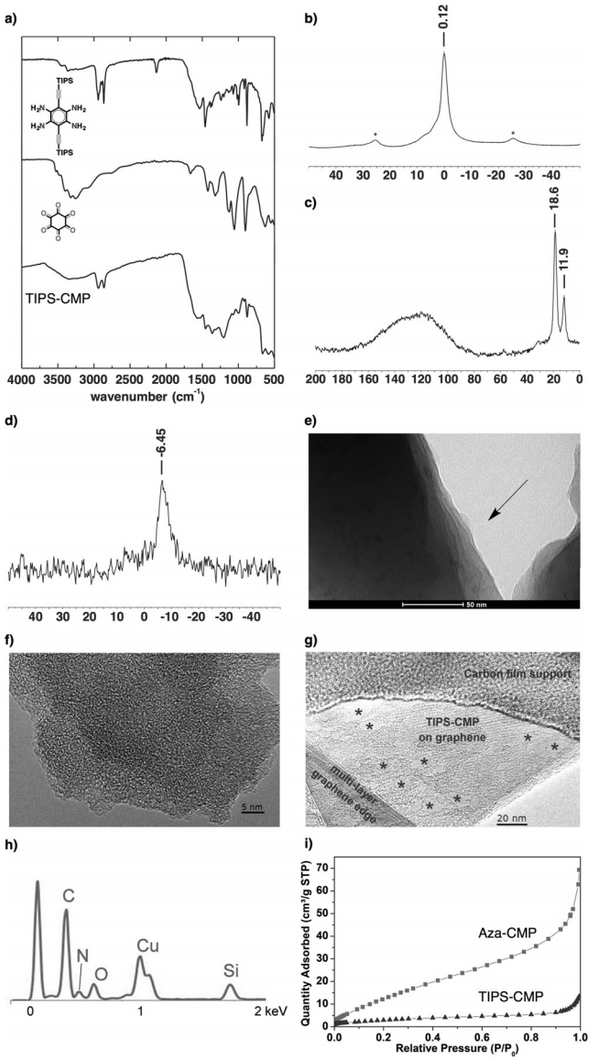

Figure 2. a) FTIR spectrum of TIPS-CMP; b) solid-state CP/MAS ^{1}H NMR spectrum of TIPS-CMP (* denotes side peaks); c) solid-state CP/MAS ^{13}C NMR spectrum of TIPS-CMP; d) ^{29}Si NMR spectrum of TIPS-CMP; e) TEM image of TIPS-CMP; f) HRTEM image of TIPS-CMP; g) HRTEM image of an individual layer of TIPS-CMP on graphene; h) EDX spectrum of TIPS-CMP (Cu peak is due to the sample holder); i) N_2 uptake of Aza-CMP and TIPS-CMP.

carbon atoms and two distinct peaks in the aliphatic region at 18.6 and 11.9 ppm corresponding to the two types of carbon atoms of the TIPS groups (Figure 2c). The ^{29}Si NMR spectrum of TIPS-CMP showed one signal at −6.45 ppm, which corresponds to the silicon atom of the TIPS groups (Figure 2d).

Transmission electron microscopy (TEM) imaging revealed layered morphologies of the TIPS-CMP material (Figures 2e; see also Figure S5) with terraces and step edges of overlapping sheets reminiscent of graphitic materials, thus confirming the 2D nature of TIPS-CMP. An irregular porous structure was discerned from high-resolution transmission electron microscopy (HRTEM) images of TIPS-CMP (Figures 2f; see also Figure S6). Importantly, individual layers of TIPS-CMP could be deposited onto graphene layers mounted on a TEM grid by dry deposition, thus providing further confirmation of the 2D nature of TIPS-CMP (Figure 2g; see also Figure S6). The individual TIPS-CMP layers showed random features reminiscent of pores (1–2 nm) and also a random distribution of larger holes (5–15 nm; marked with asterisks to guide the eye). The latter have been ascribed to defects that are expected to contain carbonyl groups in line with EDX, which evidenced the presence of O in addition to the expected C, N, and Si signals (Figure 2h). These random features are consistent with the X-ray powder diffractograms of TIPS-CMP, which showed no reflections (see Figure S7). As expected, almost negligible N_2 uptake, as illustrated by a Brunauer–Emmett–Teller (BET) surface area of 12 $m^2 g^{-1}$, was observed for TIPS-CMP. This BET surface area is about five times lower than that observed for Aza-CMP (Figure 2i), in strong agreement with the presence of six TIPS groups within the pores of TIPS-CMP, which substantially reduce the effective porosity in comparison to Aza-CMP.

To obtain a clear view of the distorted nature of TIPS-CMP, we calculated the structure of a closed pore (Figure 1). Owing to the size of the pore, calculations were performed with semiempirical models benchmarked against the crystal structure of twisted-HATNA,[13] which corresponds structurally to an angular fragment of TIPS-CMP. Different semiempirical Hamiltonians were investigated, namely, AM1, PM6, PM6-DH2, and PM7, and compared with the crystal structure of twisted-HATNA (see the Supporting Information). PM6-DH2 was selected, as it reproduces with higher accuracy the twist angle between blades (65°) of the crystal structure of twisted-HATNA (67°), thus providing even better results than previous calculations[13] at the DFT level (63°). The PM6-DH2 studies revealed that the interacting TIPS substituents force the framework of TIPS-CMP to deviate from planarity to adopt an asymmetrical propeller-like structure at each joint (Figure 1a) with an alternating disposition of the TIPS substituents above and below the plane. Twist angles between blades[16] of 95, 65, 63, 90, 74, and 72° were calculated within the pore (average twist angle: 76°). Remarkably, TIPS-CMP exhibits a maximum twist angle of 95°, which is substantially higher than the highest twist angles reported for twisted-HATNA[13] (67°). This large twist angle can be explained in terms of the higher degree of crowding within the pore as a result of the presence of six interacting TIPS substituents versus the two interacting TIPS groups in twisted-HATNA.

Remarkably, TIPS-CMP was readily dispersible in a variety of solvents. Golden-brownish dispersions, transparent to the naked eye, with concentrations in the order of 0.20 mg mL^{-1} (Figure 3a) were obtained in trifluoroacetic acid (TFA), an organic solvent commonly used to dissolve unsubstituted nitrogenated polycyclic aromatic hydrocarbons.[17] Dynamic light scattering (DLS) showed that these dispersions consisted of a distribution of particles with a hydrodynamic diameter of 180 nm, which did not change upon dilution (Figure 3b). TIPS-CMP could be also dispersed in *N*,*N*′-dimethylformamide (DMF) at lower concentrations (0.02 mg mL^{-1}), which could be increased (0.15 mg mL^{-1}) by

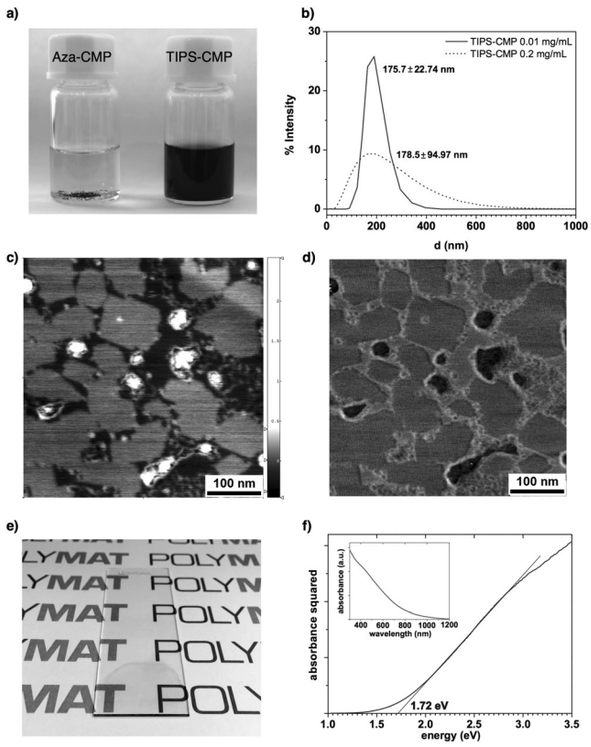

Figure 3. a) Dispersions of Aza-CMP and TIPS-CMP in TFA; b) DLS of dispersions of TIPS-CMP in TFA; c) height (range: 2.992 nm) and d) phase AFM images of a dispersion of TIPS-CMP in H_2O/EtOH (1:1); e) drop-cast thin film of TIPS-CMP from a dispersion in DMF/TFA (95:5); f) Tauc plot of the TIPS-CMP thin film (inset shows the absorption trace of the thin film).

adding a small amount of TFA (5%) to DMF. Moreover, TIPS-CMP was found to form homogeneous dispersions in H_2O/EtOH (1:1), which gave rise to individual layers that coexisted with a small fraction of larger aggregates, as observed by AFM (Figure 3c,d). The deposited dispersions on highly oriented pyrolytic graphite showed exfoliated TIPS-CMP monolayers with an average diameter of approximately 200 nm for the highest fraction of layers, which agrees with the hydrodynamic diameter observed by DLS measurements. For example, the area distribution of the largest fraction of layers falls between 4000 and 12000 nm^2 from a total of 84 layers measured (see Figure S10), but remarkably, areas as large as 28000 nm^2 were observed. From height measurements carried out on diluted dispersions, a height of 6.20 Å was observed for an individual monolayer (see Figure S10). This value is roughly double the interlayer distance of graphite, 3.35 Å, and is due to the bulky TIPS groups beneath and above the 2D aromatic moiety, which act as scaffolds with respect to the surface (Figure 1). A comparable height (7.72 Å) was obtained by modeling the adsorption of the molecular analogue of TIPS-CMP on graphite (see Figure S12). On the other hand, Aza-CMP could not be dispersed in any of the solvents or solvent mixtures mentioned above or in *N*-methylpyrrolidone (NMP), which is used for the sonication-assisted exfoliation of graphene.

Homogeneous, coherent, and optically transparent golden-brownish thin films were obtained by drop casting a dispersion of TIPS-CMP in DMF/TFA (95:5) on glass slides (Figure 3e), which enabled the estimation of the energy gap of TIPS-CMP by the Tauc[18] method (Figure 3f). The estimated energy gap of 1.7 eV for TIPS-CMP falls within the values considered for semiconductors,[19] and aligns well with the DFT value (2.1 eV) estimated for an individual pore (see the Supporting Information).

Since TIPS-CMP can form homogeneous and stable dispersions that allow liquid processing, and as a proof of concept, we tested their potential application as electrocatalysts for the ORR, in which N-doped carbon nanomaterials have shown outstanding performance.[4] For this purpose, we drop cast 50 µL of a freshly prepared dispersion of TIPS-CMP (0.2 mg mL^{-1}) in TFA directly on a glassy-carbon rotating-disk electrode (catalyst loading: 140 µg cm^{-2}) and investigated the ORR in ultrapure 0.1 M aqueous KOH. The cyclic voltammogram of an argon-saturated KOH solution shows a featureless curve. Conversely, the cyclic voltammograms of TIPS-CMP in O_2-saturated KOH clearly showed the onset of cathodic current as a result of the ORR at 0.75 V (vs. RHE), which is 150 mV more positive (i.e. less energy-consuming) than the bare glassy-carbon electrode[20,21] (Figure 4a; see Figure S13) and highlights the catalytic performance of TIPS-CMP. The voltammetric response is highly stable, as can be seen in the reverse scans, which almost match the forward scans at low scan rates (10 mV s^{-1}, as also confirmed by a time-dependent study (see Figure S14)).

The ORR performance of TIPS-CMP (with $E_{1/2} = 0.65$ V vs. NHE) is in line with that observed in current state-of-the-art organic frameworks and even superior in many cases (e.g. g-C_3N_4, C-COP-P, and C-COP-T).[22] Remarkably, whereas other organic frameworks[22] require an additional carbonization step or need to be mixed with different carbonaceous

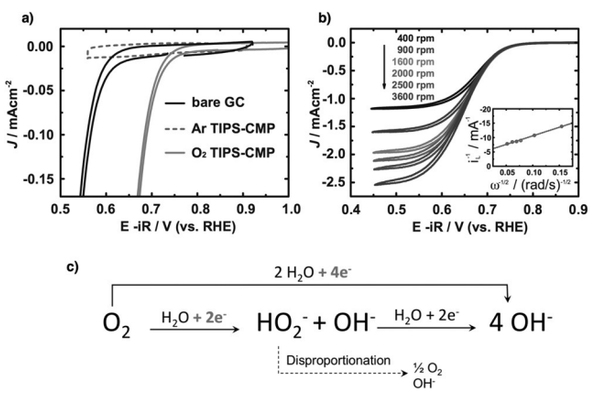

Figure 4. a) Cyclic voltammograms of a bare GC electrode (O_2-saturated) and after TIPS-CMP drop-casting (Ar-saturated and O_2-saturated) in aqueous ultrapure 0.1 M KOH (scan rate: 10 mV s^1, rotating speed: 1600 rpm). b) Cyclic voltammograms of a drop-casted TIPS-CMP on GC electrode at different rotating speeds in O_2-saturated aqueous 0.1 M KOH (inset: Koutecky—Levich analysis of the limiting currents measured at 0.55 V). c) Possible ORR mechanisms in alkaline solution, with the two- and four-electron reaction pathways highlighted. RHE = reversible hydrogen electrode.

supports to reach their level of ORR performance, TIPS-CMP does not require any post-processing to attain its electrocatalytic activity. To understand the mechanism involved in the ORR with TIPS-CMP, we studied the process further with a rotating-disk electrode at different rotation speeds (Figure 4b). By representing the limiting current as a function of the rotation speed, the number of electrons exchanged in the ORR process can be estimated by the slope of the fitting line (known as Koutecky–Levich analysis). As shown in Figure 4c, two ORR mechanisms might occur, the two-electron (from O_2 to H_2O_2) and four-electron (from O_2 to H_2O) reaction pathways. The Koutecky–Levich plot for TIPS-CMP shows a three-electron process for ORR, thus pointing to the formation of both hydrogen peroxide and water as reaction products.[4]

We have demonstrated that the flat structure of 2D aromatic frameworks can be twisted by overcrowding the nodes of the framework with bulky and rigid TIPS substituents. Twist angles as large as 95° were estimated for TIPS-CMP; they exceed substantially those previously observed for the parent twisted-HATNA.[13] TIPS-CMP was found to form homogeneous dispersions upon sonication in a range of solvents, in which it underwent spontaneous exfoliation into individual layers with an average diameter of approximately 200 nm, as observed by AFM and DLS. The enhanced dispersibility observed for TIPS-CMP has been attributed to the highly distorted aromatic framework, which results in diminished interlayer interactions that favor the exfoliation and dispersion of individual layers in organic media. Homogeneous, coherent, and optically transparent thin films were readily obtained by drop casting such dispersions. UV/Vis absorption spectroscopy of such films illustrated the semiconducting nature of TIPS-CMP (energy gap: 1.7 eV). TIPS-CMP modified electrodes prepared by drop casting showed enhanced ORR electrocatalytic activity (+150 mV) in comparison to the bare GC electrode without the need for any additional post-processing step. Overall, this study shows that twisting is a very powerful strategy to enhance the dispersibility and processability of conjugated materials consisting of fused aromatic rings, even for systems that span hundreds of nanometers in two dimensions, thus opening the door to the formulation of CMPs into inks to enable large-area and low-cost liquid-deposition methods.

Acknowledgements

We are grateful to the Basque Science Foundation for Science (Ikerbasque), POLYMAT, the University of the Basque Country (SGIker), the Deutsche Forschungsgemeinschaft (AU 373/3-1 and MA 5215/4-1), Gobierno de España/FEDER (Ministerio de Economía y Competitividad, CTQ2015-71936-REDT, CTQ2016-77970-R, and ENE2015-66975-C3), Gobierno Vasco (BERC program, PC2015-1-01(06-37), and IT1069-16), Diputacioń Foral de Guipuzkoa (2015-CIEN-000054-01), CICECO—Aveiro Institute of Materials, POCI-01-0145-FEDER-007679 (FCT ref. UID/CTM/50011/ 2013), ON2 (NORTE-07–0162-FEDER-000086), the Fund of Scientific Research—Flanders (FWO), the Internal Funds KU Leuven, the Belgian Federal Science Policy Office (IAP-7/05), and the Nanoscale and Microscale Research Centre (NMRC, University of Nottingham, UK) for access to TEM. We have received funding for the research leading to these results from the European Union Seventh Framework Programme as a European Research Area Action (ERA-Chemistry) and a Marie Curie Action (Career Integration Grant No. 618247) and from the European Union Framework Programme for Research and Innovation Horizon 2020 as a Future and Emerging Technologies Action (FET Open) under Grant Agreement No. 664878 (2D-INK).

Conflict of interest

The authors declare no conflict of interest.

Keywords: carbon nanostructures · materials science · nanocarbons · organic frameworks · twisted aromatic systems

How to cite: *Angew. Chem. Int. Ed.* **2017**, *56*, 6946–6951
Angew. Chem. **2017**, *129*, 7050–7055

[1] a) K. S. Novoselov, A. K. Geim, S. V. Morozov, D. Jiang, Y. Zhang, S. V. Dubonos, I. V. Grigorieva, A. A. Firsov, *Science* **2004**, *306*, 666–669; b) E. Vázquez, F. Giacalone, M. Prato, *Chem. Soc. Rev.* **2014**, *43*, 58–69; c) M. Quintana, E. Vazquez, M. Prato, *Acc. Chem. Res.* **2013**, *46*, 138–148; d) S. Eigler, A. Hirsch, *Angew. Chem. Int. Ed.* **2014**, *53*, 7720–7738; *Angew. Chem.* **2014**, *126*, 7852–7872; e) A. Hirsch, J. M. Englert, F. Hauke, *Acc. Chem. Res.* **2013**, *46*, 87–96; f) J. Malig, N. Jux, D. M. Guldi, *Acc. Chem. Res.* **2013**, *46*, 53–64; g) L. Rodríguez-Pérez, M. A. Herranz, N. Martín, *Chem. Commun.* **2013**, *49*, 3721–3735.

[2] a) Y. Xu, S. Jin, H. Xu, A. Nagai, D. Jiang, *Chem. Soc. Rev.* **2013**, *42*, 8012–8031; b) J. W. Colson, W. R. Dichtel, *Nat. Chem.* **2013**, *5*, 453–465; c) J.-J. Adjizian, P. Briddon, B. Humbert, J.-L. Duvail, P. Wagner, C. Adda, C. Ewels, *Nat. Commun.* **2014**, *5*, 5842; d) G. Zhu, H. Ren, *Porous Organic Frameworks. Design, Synthesis and Their Advanced Applications*, Springer, **2015**; e) A. G. Slater, A. I. Cooper, *Science* **2015**, *348*, aaa8075; f) K. Sakaushi, M. Antonietti, *Acc. Chem. Res.* **2015**, *48*, 1591–1600; g) P. J. Waller, F. Gándara, O. M. Yaghi, *Acc. Chem. Res.* **2015**, *48*, 3053–3063; h) Z. Xiang, D. Cao, L. Dai, *Polym. Chem. Polymer Chem.* **2015**, *6*, 1896–1911; i) U. Díaz, A. Corma, *Coord. Chem. Rev.* **2016**, *311*, 85–124; j) J. L. Segura, M. J. Mancheno, F. Zamora, *Chem. Soc. Rev.* **2016**, *45*, 5635–5671; k) R. Dong, M. Pfeffermann, H. Liang, Z. Zheng, X. Zhu, J. Zhang, X. Feng, *Angew. Chem. Int. Ed.* **2015**, *54*, 12058–12063; *Angew. Chem.* **2015**, *127*, 12226–12231; l) T. Kambe, R. Sakamoto, K. Hoshiko, K. Takada, M. Miyachi, J.-H. Ryu, S. Sasaki, J. Kim, K. Nakazato, M. Takata, H. Nishihara, *J. Am. Chem. Soc.* **2013**, *135*, 2462–2465.

[3] a) Y. Kou, Y. Xu, Z. Guo, D. Jiang, *Angew. Chem. Int. Ed.* **2011**, *50*, 8753–8757; *Angew. Chem.* **2011**, *123*, 8912–8916; b) J. Guo, Y. Xu, S. Jin, L. Chen, T. Kaji, Y. Honsho, M. A. Addicoat, J. Kim, A. Saeki, H. Ihee, S. Seki, S. Irle, M. Hiramoto, J. Gao, D. Jiang, *Nat. Commun.* **2013**, *4*, 2736; c) J. Mahmood, E. K. Lee, M. Jung, D. Shin, I.-Y. Jeon, S.-M. Jung, H.-J. Choi, J.-M. Seo, S.-Y. Bae, S.-D. Sohn, N. Park, J. H. Oh, H.-J. Shin, J.-B. Baek, *Nat. Commun.* **2015**, *6*, 6486; d) J. Mahmood, E. K. Lee, M. Jung, D. Shin, H.-J. Choi, J.-M. Seo, S.-M. Jung, D. Kim, F. Li, M. S. Lah,

N. Park, H.-J. Shin, J. H. Oh, J.-B. Baek, *Proc. Natl. Acad. Sci. USA* **2016**, *113*, 7414 – 7419.
[4] a) L. Dai, Y. Xue, L. Qu, H.-J. Choi, J.-B. Baek, *Chem. Rev.* **2015**, *115*, 4823 – 4892; b) K. Sakaushi, T.-P. Fellinger, M. Antonietti, *ChemSusChem* **2015**, *8*, 1156 – 1160.
[5] Y. Zheng, Y. Jiao, Y. Zhu, L. H. Li, Y. Han, Y. Chen, A. Du, M. Jaroniec, S. Z. Qiao, *Nat. Commun.* **2014**, *5*, 3783.
[6] a) X. Zhang, L. Hou, A. Ciesielski, P. Samorì, *Adv. Energy Mater.* **2016**, DOI: 10.1002/aenm.201600671; b) X. Peng, L. Peng, C. Wu, Y. Xie, *Chem. Soc. Rev.* **2014**, *43*, 3303 – 3323.
[7] L. Peng, Y. Zhu, D. Chen, R. S. Ruoff, G. Yu, *Adv. Energy Mater.* **2016**, DOI: 10.1002/aenm.201600025.
[8] F. Bonaccorso, A. Bartolotta, J. N. Coleman, C. Backes, *Adv. Mater.* **2016**, *28*, 6136 – 6166.
[9] a) I. Berlanga, M. L. Ruiz-González, J. M. González-Calbet, J. L. G. Fierro, R. Mas-Ballesté, F. Zamora, *Small* **2011**, *7*, 1207 – 1211; b) S. Chandra, S. Kandambeth, B. P. Biswal, B. Lukose, S. M. Kunjir, M. Chaudhary, R. Babarao, T. Heine, R. Banerjee, *J. Am. Chem. Soc.* **2013**, *135*, 17853 – 17861.
[10] D. N. Bunck, W. R. Dichtel, *J. Am. Chem. Soc.* **2013**, *135*, 14952 – 14955.
[11] S. Mitra, S. Kandambeth, B. P. Biswal, A. Khayum M., C. K. Choudhury, M. Mehta, G. Kaur, S. Banerjee, A. Prabhune, S. Verma, S. Roy, U. K. Kharul, R. Banerjee, *J. Am. Chem. Soc.* **2016**, *138*, 2823 – 2828.
[12] M. A. Khayum, S. Kandambeth, S. Mitra, S. B. Nair, A. Das, S. S. Nagane, R. Mukherjee, R. Banerjee, *Angew. Chem. Int. Ed.* **2016**, *55*, 15604 – 15608; *Angew. Chem.* **2016**, *128*, 15833 – 15837.
[13] S. Choudhary, C. Gozalvez, A. Higelin, I. Krossing, M. Melle-Franco, A. Mateo-Alonso, *Chem. Eur. J.* **2014**, *20*, 1525 – 1528.
[14] a) G. Tregnago, C. Fléchon, S. Choudhary, C. Gozalvez, A. Mateo-Alonso, F. Cacialli, *Appl. Phys. Lett.* **2014**, *105*, 143304; b) D. Cortizo-Lacalle, A. Pertegas, L. Martinez-Sarti, M. Melle-Franco, H. J. Bolink, A. Mateo-Alonso, *J. Mater. Chem. C* **2015**, *3*, 9170 – 9174; c) S. More, S. Choudhary, A. Higelin, I. Krossing, M. Melle-Franco, A. Mateo-Alonso, *Chem. Commun.* **2014**, *50*, 1976 – 1979; d) R. A. Pascal, Jr., *Chem. Rev.* **2006**, *106*, 4809 – 4819; e) A. Mateo-Alonso, *Chem. Soc. Rev.* **2014**, *43*, 6311 – 6324; f) M. Ball, Y. Zhong, Y. Wu, C. Schenck, F. Ng, M. Steigerwald, S. Xiao, C. Nuckolls, *Acc. Chem. Res.* **2015**, *48*, 267 – 276.
[15] C. An, X. Guo, M. Baumgarten, *Cryst. Growth Des.* **2015**, *15*, 5240 – 5245.
[16] Herein, the term "twist angle between blades" refers to the torsion angle between atoms A, B, C, and D.

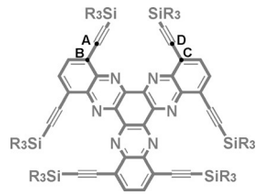

[17] A. Mateo-Alonso, N. Kulisic, G. Valenti, M. Marcaccio, F. Paolucci, M. Prato, *Chem. Asian J.* **2010**, *5*, 482 – 485.
[18] J. Tauc, *Mater. Res. Bull.* **1968**, *3*, 37 – 46.
[19] Given the similar pK_a values of TFA (0.23) and pyrazine (0.36), and also the high volatility of TFA as compared to DMF, we can safely assume that the films were neutral after overnight vacuum drying.
[20] The onset of cathodic current as a result of the ORR is 120 mV more negative than a standard Pt/C electrode (Pt 5%).
[21] T. J. Schmidt, H. A. Gasteiger, G. D. Stäb, P. M. Urban, D. M. Kolb, R. J. Behm, *J. Electrochem. Soc.* **1998**, *145*, 2354 – 2358.
[22] a) S. M. Lyth, Y. Nabae, S. Moriya, S. Kuroki, M.-a. Kakimoto, J.-i. Ozaki, S. Miyata, *J. Phys. Chem. C* **2009**, *113*, 20148 – 20151; b) Y. Zheng, Y. Jiao, J. Chen, J. Liu, J. Liang, A. Du, W. Zhang, Z. Zhu, S. C. Smith, M. Jaroniec, G. Q. Lu, S. Z. Qiao, *J. Am. Chem. Soc.* **2011**, *133*, 20116 – 20119; c) Z. Xiang, D. Cao, L. Huang, J. Shui, M. Wang, L. Dai, *Adv. Mater.* **2014**, *26*, 3315 – 3320; d) Z. Xiang, Y. Xue, D. Cao, L. Huang, J.-F. Chen, L. Dai, *Angew. Chem. Int. Ed.* **2014**, *53*, 2433 – 2437; *Angew. Chem.* **2014**, *126*, 2465 – 2469; e) S. Yang, X. Feng, X. Wang, K. Müllen, *Angew. Chem. Int. Ed.* **2011**, *50*, 5339 – 5343; *Angew. Chem.* **2011**, *123*, 5451 – 5455.

Manuscript received: January 10, 2017
Version of record online: March 20, 2017

Angewandte Chemie
Eine Zeitschrift der Gesellschaft Deutscher Chemiker

Supporting Information

Twisted Aromatic Frameworks: Readily Exfoliable and Solution-Processable Two-Dimensional Conjugated Microporous Polymers

*A. Belen Marco, Diego Cortizo-Lacalle, Iñigo Perez-Miqueo, Giovanni Valenti, Alessandro Boni, Jan Plas, Karol Strutyński, Steven De Feyter, Francesco Paolucci, Mario Montes, Andrei N. Khlobystov, Manuel Melle-Franco, and Aurelio Mateo-Alonso**

anie_201700271_sm_miscellaneous_information.pdf

1. Materials and Methods

Reagents for synthesis were, if not otherwise specified, purchased from Aldrich, Fluka or Acros. Commercial chemicals and solvents were used as received. 5,6-dinitro-4,7-bis((triisopropylsilyl)ethynyl)benzo[c][1,2,5]thiadiazole[1] was synthesized according to the reported procedure.

THF, DMF and Toluene were dried using an Innovative Pure Solve solvent purification system.

Analytical thin layer chromatography (TLC) was done using aluminum sheets (20x20 cm) pre-coated with silica gel RP-18W 60 F254 from Merck.

Column chromatography was carried out using Silica gel 60 (40-60 μm) from Scharlab.

Solid-State ^{1}H and ^{13}C/CP MAS NMR spectra were recorded on a Bruker Avance III 400 MHz NMR spectrometer at a MAS rate of 12 kHz and a CP contact time of 2 ms. NMR spectra in solution were recorded on a Bruker Avance 400 MHz spectrometer at 298 K using partially deuterated solvents as internal standards. Coupling constants (*J*) are denoted in Hz and chemical shifts (δ) in ppm. Multiplicities are denoted as follows: s = singlet, d = doublet, t = triplet, m = multiplet, br = broad.

ATR-FTIR spectra were recorded on a Bruker ALPHA ATR-IR spectrometer.

Elemental analysis was carried out in a Euro EA Elemental Analyzer from EuroVector.

UV-vis-NIR were performed in a Perkin-Elmer Lambda 950 spectrometer

The pore structure was evaluated by nitrogen sorption isotherms, measured at 77 K with a Micromeritics ASAP 2020 Physisorption Analyzer. Before measurement, the samples were degassed in vacuum at 230 °C for 10 h. The Brunauer-Emmett-Teller (BET) method was used to calculate the specific surface areas.

Transmission Electron Microscopy was performed using a TECNAI G2 20 TWIN (FEI), operating at an accelerating voltage of 200 KeV in a bright-field image mode. Samples were prepared by deposition of the molten solids on a carbon film copper grid. HRTEM analysis was performed on a JEOL2100 FEG microscope. The imaging conditions

were carefully tuned by lowering the accelerating voltage of the microscope to 100 kV and reducing the beam current density to a minimum. The sample (ca. 0.1 mg) was dispersed in methanol (2 mL) using an ultrasonic bath and deposited onto a lacey carbon film coated TEM copper grid. The morphology of the film was determined by taking micrographs of 100 nm^2 areas from different regions of the specimen, and the nano scale features were imaged using high resolution imaging of 20 nm^2 areas.

The X-ray powder diffraction patterns were collected by using a PHILIPS X'PERT PRO automatic diffractometer operating at 40 kV and 40 mA, in theta-theta configuration, secondary monochromator with Cu-Kα radiation (λ = 1.5418 Å) and a PIXcel solid state detector (active length in 2θ 3.347º). Data were collected from 3 to 80° 2θ (step size = 0.026 and time per step = 0.150 s) at room temperature. An automatic divergence slit was used, giving a constant irradiated length of 4.0 mm illumination.

Thermogravimetric analysis was performed in a TGA Q500 from TA Instruments under nitrogen with a heating rate of 10 ^{o}C/min. Air was introduced at 800 ^{o}C.

All AFM measurements were performed with a Bruker MultiMode 8 microscope in tapping mode, using AC-160-TS tips from Olympus. Samples were prepared by dropcasting few drops of a H_2O/EtOH 1:1 dispersion on highly oriented pyrolytic graphite (HOPG). The solvent was allowed to evaporate prior to imaging.

The electrochemical properties have been evaluated in a three-electrode electrochemical cell using a glassy carbon (GC) rotating disk electrode (RDE, Tacussel, France) as support for the deposition of the catalyst dispersion, a SCE reference electrode and a Pt mesh auxiliary electrode. The electrochemistry work stations used for the entire characterization was a SP-300 bipotentiostat (Biologic Instruments), having an additional current booster and a built-in impedance analyser.

2. Synthesis of Aza-CMP and TIPS-CMP.

Synthesis of Aza-CMP:

To a schlenk flask with hexaketocyclohexane octahydrate (124.8 mg, 0.4 mmol) and 1,2,4,5-benzenetetraamine chlorohydrate (170.4 mg, 0.6 mmol), a mixture of dioxane/acetic acid (1:4 v/v, 20 mL) was added. The mixture was sonicated for five minutes, and subsequently degassed by three cycles of freeze-pump-thaw. Once finished the degassing process, the mixture was heated at 135 ^{o}C and stirred for 7 days under nitrogen. After this time, reaction was cooled to room temperature and filtered off, washing the resulting dark solid with water, HCl aq. 0.2N, methanol and THF. The solid was Soxhlet extracted with water (48 h), methanol (48 h), THF (48 h) and CH_2Cl_2 (48 h). The compound was then sonicated in the presence of methanol (20 minutes), THF (20 minutes), CH_2Cl_2 (20 minutes) and Et_2O (20 minutes), before being dried under vacuum at 150 ^{o}C for 24 hours, yielding **Aza-CMP** as a black solid (73 mg, 68%). SS-^{1}H-NMR (δ) (ppm): 7.24. SS-^{13}C-NMR (δ) (ppm): 170-76, 131, 111. ATR-FTIR (cm^{-1}): 3001 (C–H, st); 1597, 1508 (C=N/C=C); 1459 (C–C, st); 1354, 1216 (C–N, st). Elemental Analysis: calculated: C (63.16%), N (29.46%) H (1.77%); observed: C (54.33%), N (22.96%) H (2.54%).

Synthesis of TIPS-CMP:

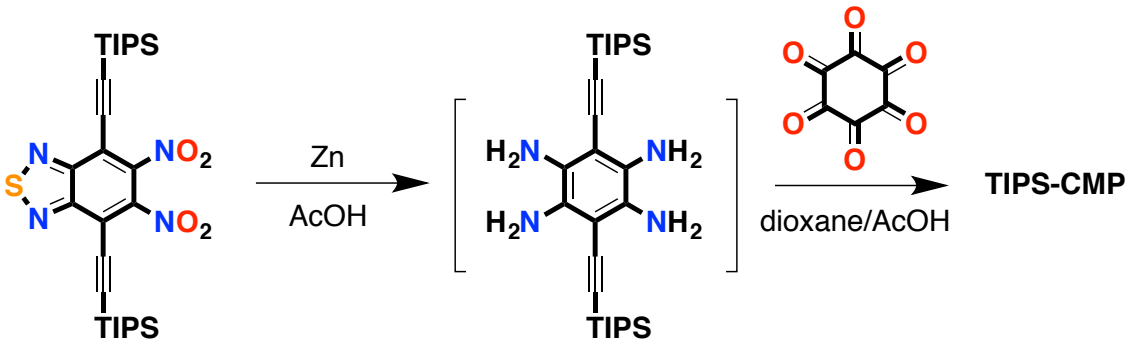

Scheme S1.

To a solution of 5,6-dinitro-4,7-bis(triisopropylsilyl(ethynyl))benzo[c][1,2,5]thiadiazole (400 mg, 0.68 mmol) in acetic acid (6 mL), zinc powder (886 mg, 13.6 mmol) was added and the mixture was stirred for 6 hours at 60 ^{o}C. After this time, reaction was cooled to room temperature and filtered off over celite, washing the solids with acetic acid (~8 mL). The filtrate was directly transferred to a Shlenk flask with hexaketocyclohexane octahydrate (71 mg, 0.68 mmol) to avoid the decomposition of

the tetraamine, and dioxane (2 mL) was added. The mixture was sonicated for five minutes, and subsequently degassed by three cycles of freeze-pump-thaw. Once finished the degassing process, the mixture was heated at 135 ^{o}C and stirred for 7 days under nitrogen. After this time, reaction was cooled to room temperature and filtered off, washing the resulting dark solid with water, HCl aq. 0.2N, methanol and THF. The solid was Soxhlet extracted with water (48 h), methanol (48 h), THF (48 h) and CH_2Cl_2 (48 h). The compound was then sonicated in the presence of methanol (20 minutes), THF (20 minutes), CH_2Cl_2 (20 minutes) and Et_2O (20 minutes), before being dried under vacuum at 150 ^{o}C for 24 hours, yielding the corresponding CMP as a black solid (41 mg, 22%). SS-^{1}H-NMR (δ) (ppm): 0.12. SS-^{13}C-NMR (δ) (ppm): 170–76 (br), 18.6, 11.9. SS-^{29}Si-NMR (δ) (ppm): –6.45. ATR-FTIR (cm^{-1}): 2940, 2861 (C–H, st); 1600, 1566, 1518 (C=N/C=C); 1454 (C–C, st); 1359, 1202 (C–N, st). Elemental Analysis: Elemental Analysis: calculated: C (69.77%), N (10.17%) H (7.93%); observed: C (49.57%), N (9.34%) H (4.27%). The observed carbon and hydrogen values are lower than the calculated on account of the formation of refractory complexes with carbon such as non-combustible silicon carbide byproducts and volatile stable silane. This behaviour has been observed for boronate ester linked COFs.[2]

3. IR Spectroscopy

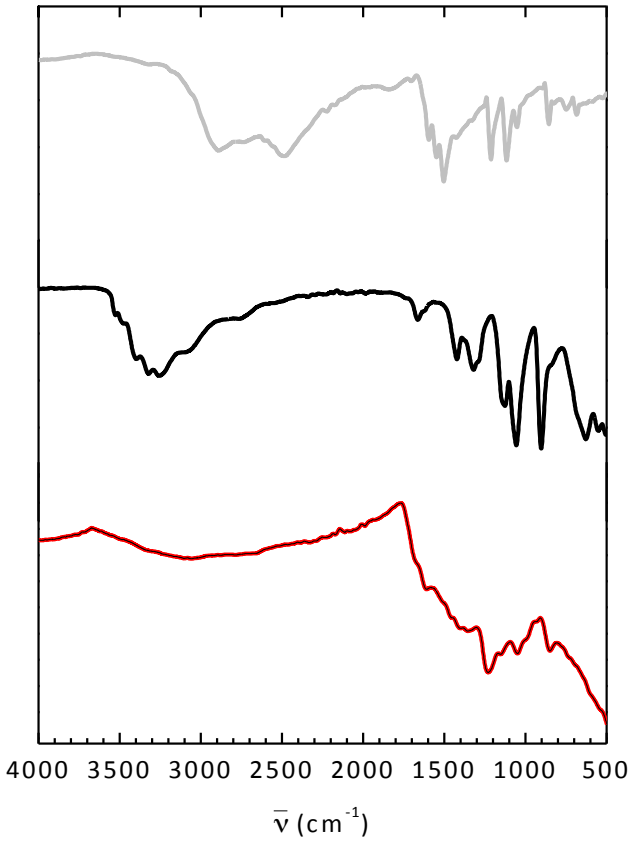

Figure S1. IR spectra of **Aza-CMP** (red) and its precursors: hexaketocyclohexane octahydrate (black) and benzenetetraamine chlorohydrate (grey).

4. Solid State-Nuclear Magnetic Resonance (SS-NMR):

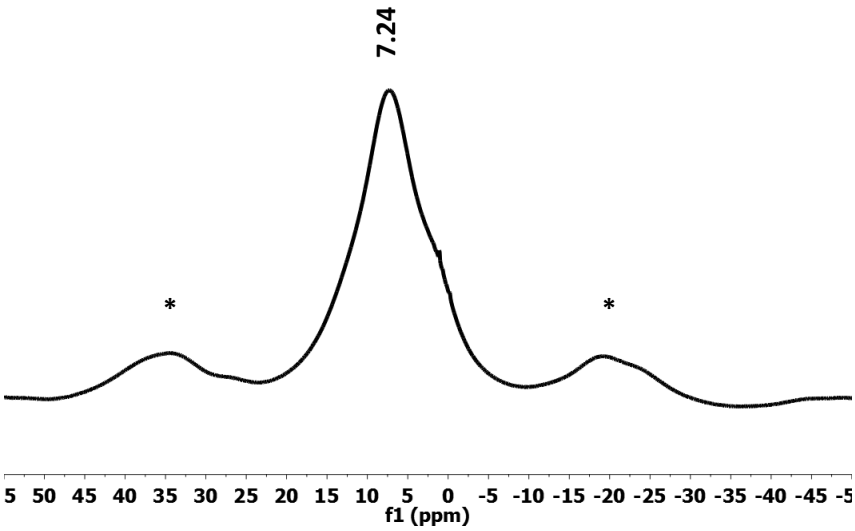

Figure S2. SS-^{1}H-NMR spectrum of **Aza-CMP**.

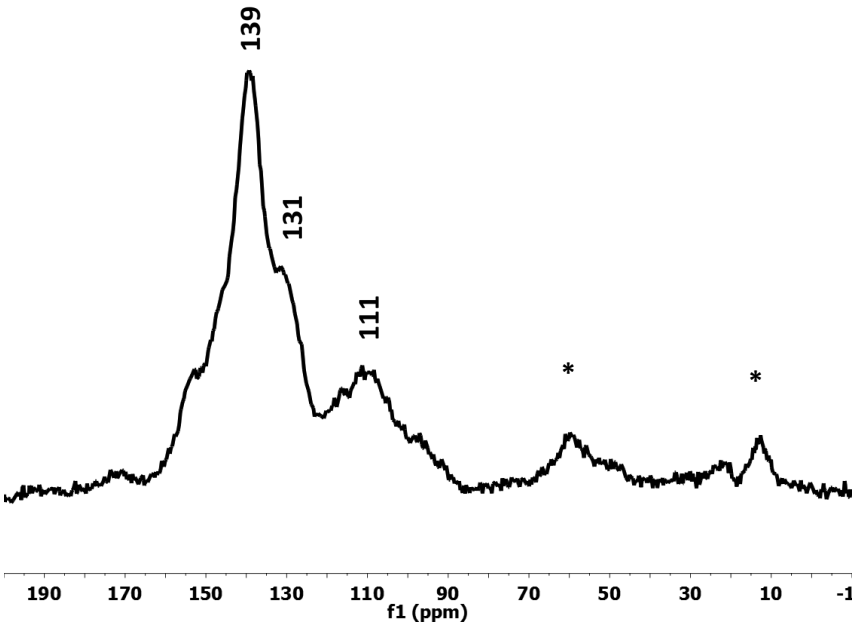

Figure S3. SS-^{13}C-NMR spectrum of **Aza-CMP**.

5. Transmission Electronic Microscopy (TEM):

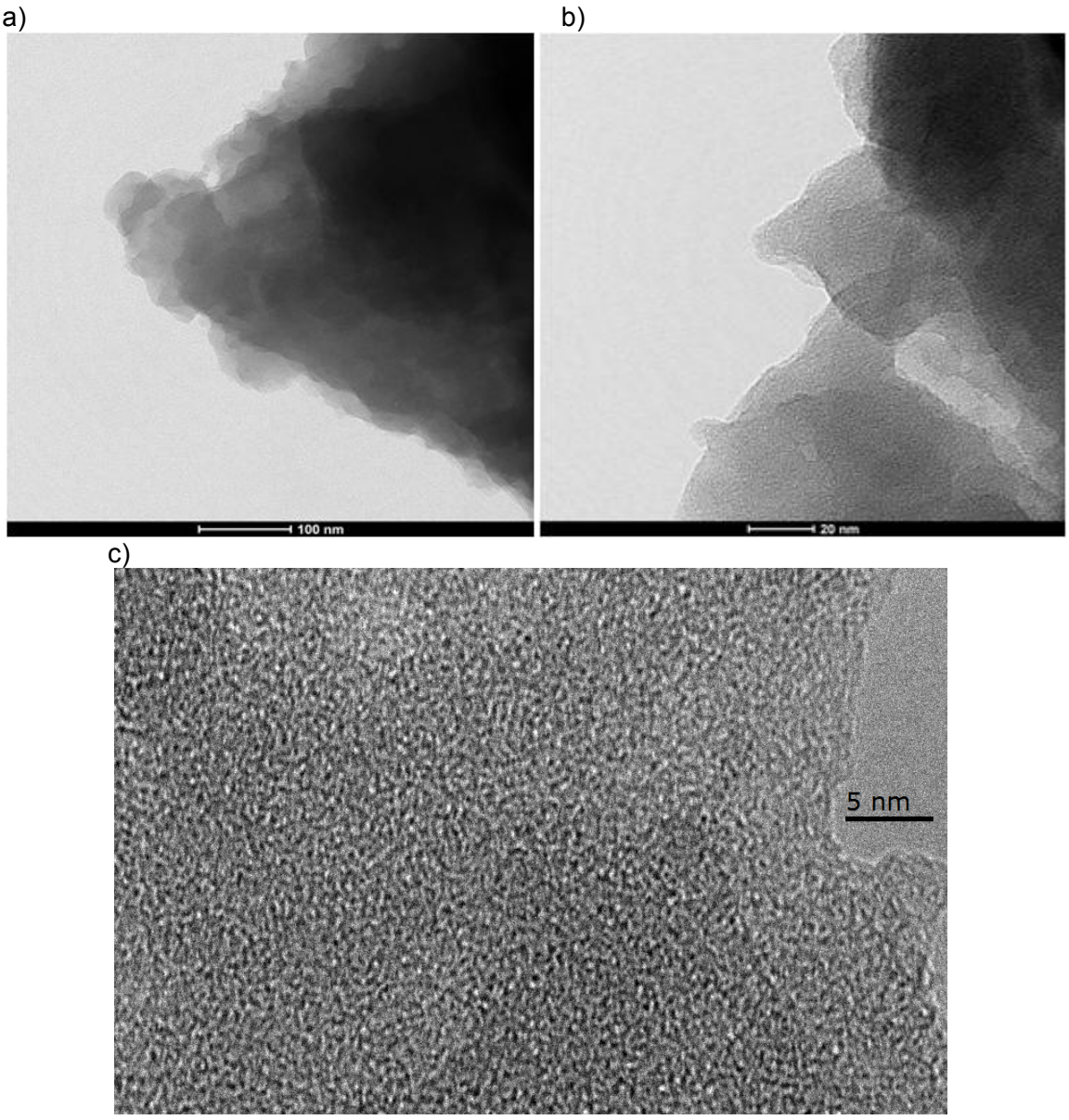

Figure S4. TEM (a and b) and and HRTEM (c) micrographs of **Aza-CMP**.

a)

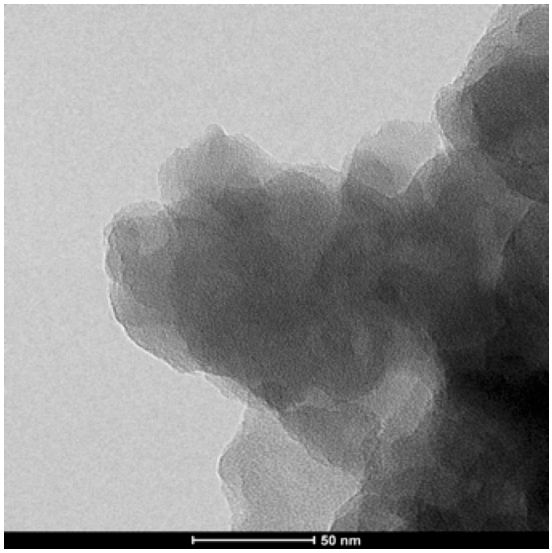

b)

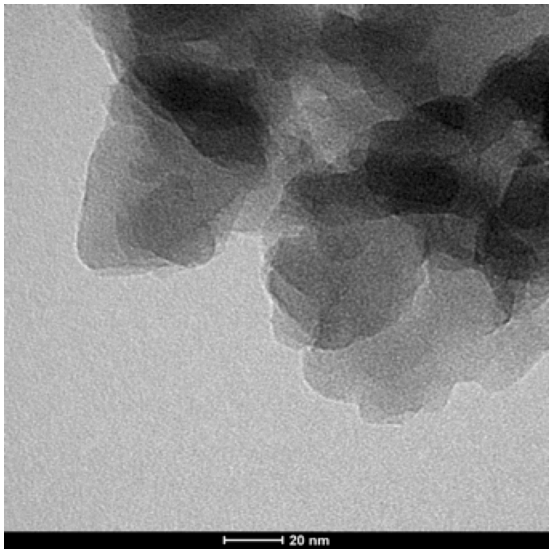

c)

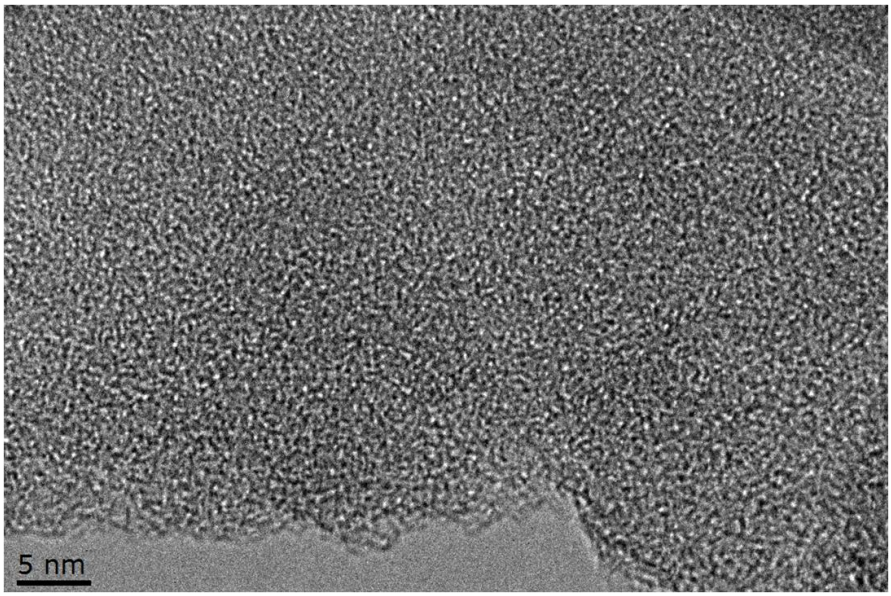

Figure S5. TEM (a and b) and and HRTEM (c) micrographs of **TIPS-CMP**.

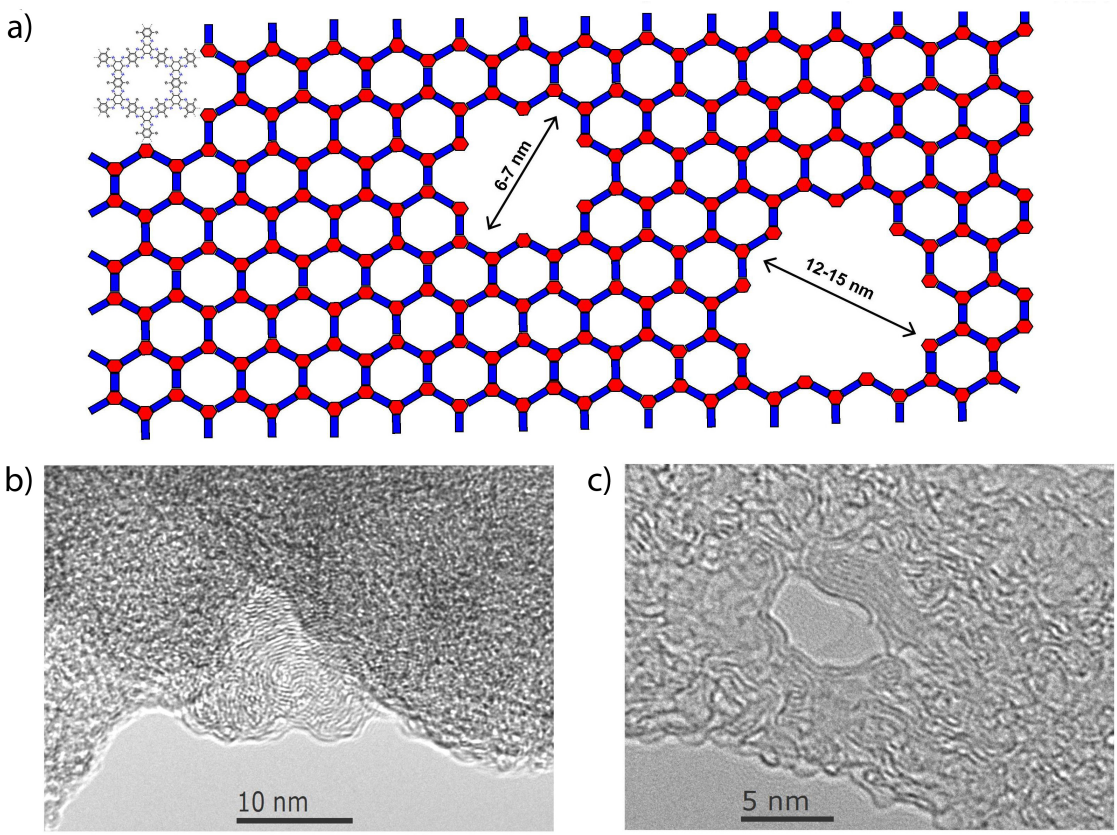

Figure S6. (a) Schematic diagram illustrating that the holes are a result of structural defects occurring in the monolayer where two or more building blocks of the hexagonal network are missing. (b and c) **TIPS-CMP**, as all covalent organic frameworks, is highly susceptible to electron beam damage during TEM imaging, such that even moderate irradiation leads to rapid degradation of the structure and transformation of **TIPS-CMP** to graphitised carbon where the graphitic layers with characteristic 0.33 nm spacing can be clearly observed.

6. Powder X-Ray Diffraction data

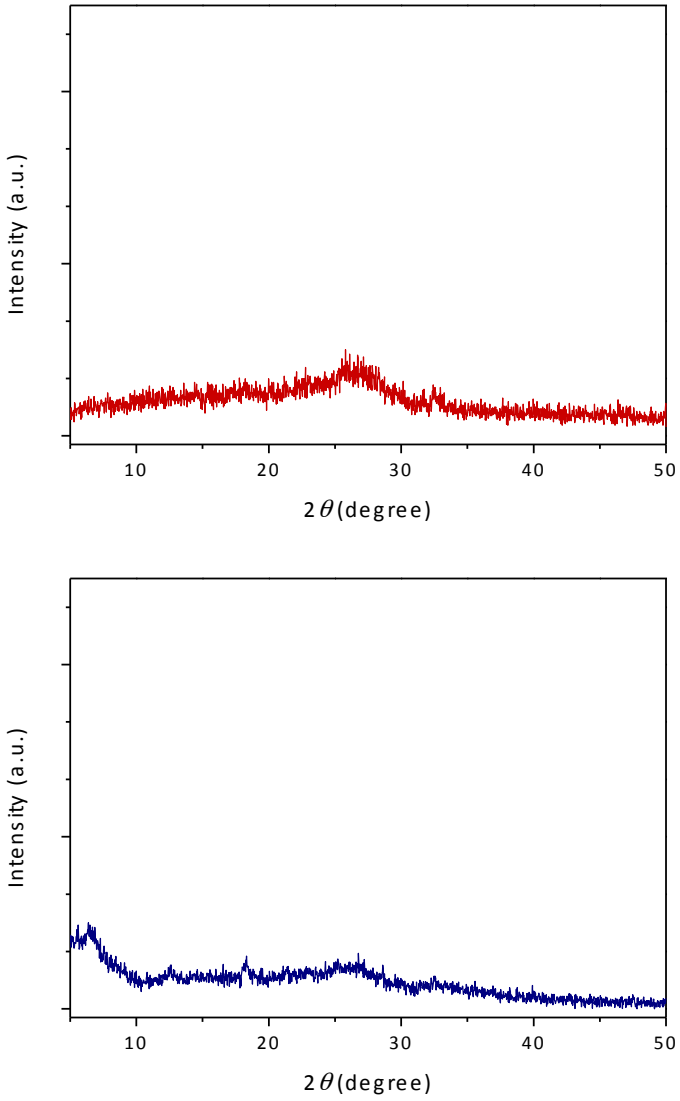

Figure S7. X-Ray powder diffraction pattern for **Aza-CMP** (top) and for **TIPS-CMP** (bottom).

7. Thermogravimetric analysis

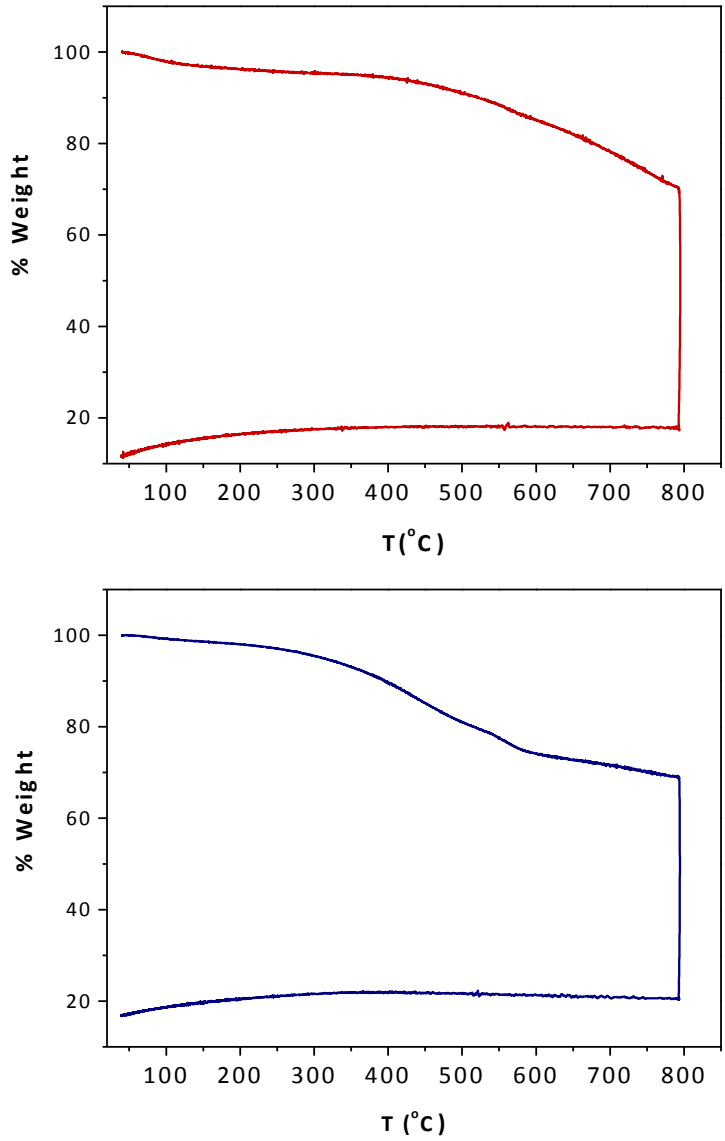

Figure S8. Thermogravimetric analysis of **Aza-CMP** (top) and of **TIPS-CMP** (bottom) performed at 10 °C/min under inert atmosphere (air was flushed after 800 °C).

8. Solubility

Solubility of CMPs was tested by adding increasing known amounts of the solids to pure trifluoroacetic acid (TFA). First, it was checked that TIPS-CMP was able to be completely dissolved in TFA in concentrations ca. 0.2 mg/mL. Then, the concentration was confirmed by adding small measured volumes of TFA until homogeneous dispersions were observed, confirming that the solubility of TIPS-CMP in TFA is 0.2 mg/mL. This process was repeated at least 10 times with reproducible results.

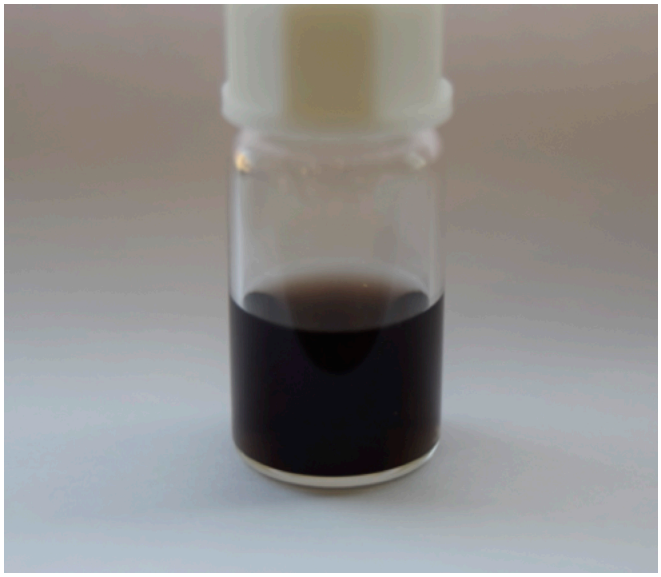

Figure S9. High-resolution picture of the TFA dispersion (0.2 mg/mL) of **TIPS-CMP**.

9. AFM studies.

0.4 mg of TIPS-CMP were sonicated in 1 ml of H_2O/EtOH (50:50) for 5 minutes and the solution started coloring black, indicating exfoliation of the flakes. The solution was sonicated for 30 minutes before dropcasting on a preheated HOPG sample (100°C) and dried for 1 minute. This sample was analysed with AFM. The size of the flakes was characterized measuring the area of individual flakes in large-scale phase images. In total, the area of 84 individual flakes was measured and the area distribution is presented in the diagram in figure S10. From this diagram, we can see that the largest fraction of flakes is that with the smallest area (up to 12000 nm²).

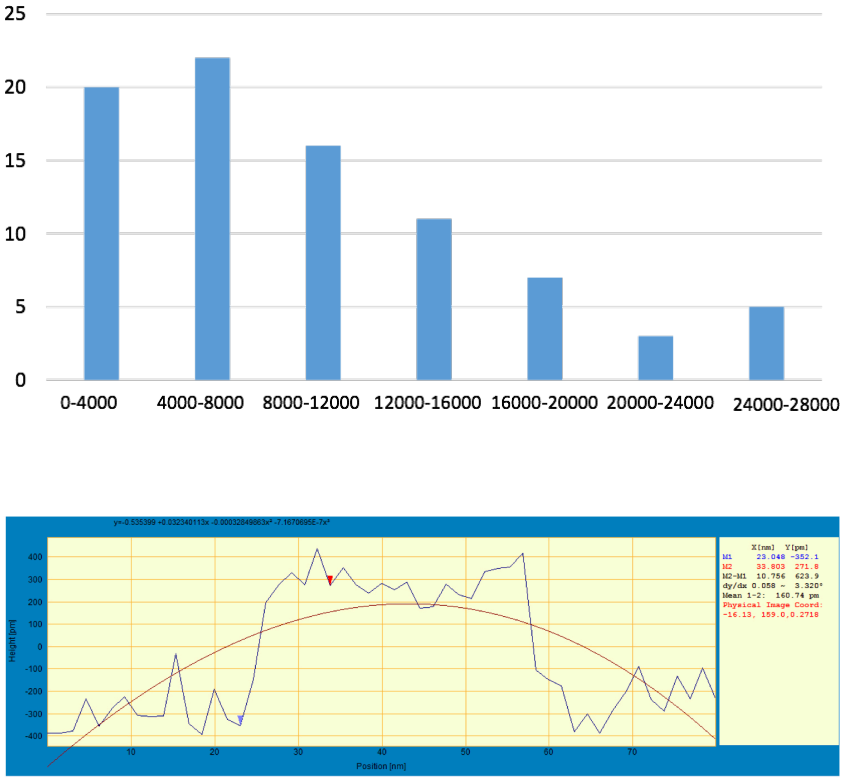

Figure S10. Size distribution of TIPS-CMP in an EtOH/water 1:1 dispersion divided in 4000 nm² intervals (top). Height estimation of an individual flake on bare HOPG (bottom).

10. Thin film deposition

Thin films of **TIPS-CMP** were prepared by drop casting a solution 0.15 mg/mL in a mixture DMF/TFA 95:5 v/v on a glass slide, and were left to dry under air in a protected environment and subsequently under vacuum to assure evaporation of DMF before recording the electronic absorption spectra.

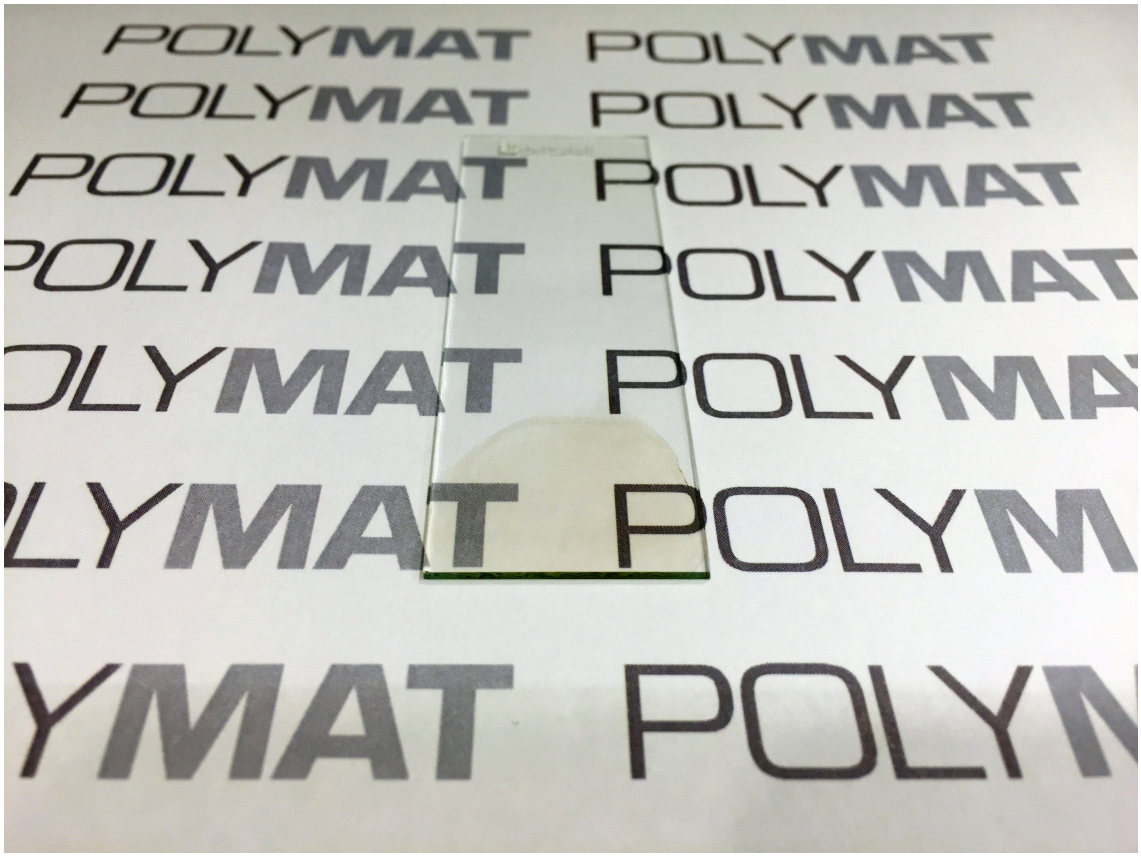

Figure S11. High-resolution pictures of the thin films prepared by drop casting a 0.15 mg/mL solution of **TIPS-CMP** in DMF:TFA 95:5 on a glass substrate.

11. Theoretical calculations

Computer models of the TIPS-CMP 2D-extended system were performed in all cases with a molecular analogue with the empirical formula $C_{372}N_{36}Si_{24}H_{516}$ containing one hexagonal pore. Three-dimensional structures were generated with the program Avogadro 1.1.1.[3] and optimized with the program MOPAC2012[4] with the PM6-DH2 semiempirical Hamiltonian.[5] Due to the large size of the molecular analogue, 948 atoms, structural simulation studies were performed with semiempirical models benchmarked against previously studied twisted molecules.[6] Different semiempirical Hamiltonians were tried, namely: AM1, PM6, PM6-DH2 and PM7, and compared with the X-ray structure and DFT models of *twisted*-HATNA. PM6-DH2 was chosen as it yielded an average twist angle between blades of 65° in better agreement with the experimental value (67°) than DFT (63°).[6]

Conformational search

In order to explore different conformations, we performed Molecular Dynamics (MD) simulations at 298 K with the molecular mechanics MMFF94 force field as implemented in the software Tinker. Collisions with solvent molecules were considered implicitly through the use of stochastic dynamics with a friction coefficient of 2 ps^{-1} to improve conformational sampling. The simulation was run for 1 ns and snapshots of the trajectory were selected at 20 ps intervals yielding 50 different conformations that were optimized at the PM6-DH2 level. All conformations in the MD simulation look very much alike and the TIPS functional groups show similar relative orientations with respect to the aromatic core (Table S1).

The “best minimum” (Table S1) corresponds to the conformer with the lowest energy at the PM6-DH2 level and shows twisting angles similar to the average values for all conformers. The table shows also the maximum and minimum relative angles and the Standard Deviation (SD) for all conformations.

The average of the average twisting angles for each conformations is shown in Table S2. The average twisting angle for each conformer oscillates between 68 (minimum) and 77 (maximum) degrees.

Table S1. Angles between adjacent branches in the inner pore (the change of sign implies that the dihedral angles are antiparallel, i.e. the branches are pointing in alternating, up and down, directions).

		angle 1	angle 2	angle 3	angle 4	angle 5	angle 6
Best minimum	1 conformer	72	-95	65	-63	90	-74
Statistics 1 ns/20 ps	Average all conformers	70	-92	60	-57	89	-70
Statistics 1 ns/20 ps	Maximum all conformers	87	-99	74	-74	101	-78
Statistics 1 ns/20 ps	Minimum all conformers	56	-84	47	-45	78	-58
Statistics 1 ns/20 ps	SD all conformers	6	4	7	7	5	4

Table S2. Average angles between adjacent branches in the inner pore.

Statistics 1 ns/20 ps	Average |angle|	73
Statistics 1 ns/20 ps	Max. ave. |angle|	77
Statistics 1 ns/20 ps	Min. ave. |angle|	68
Statistics 1 ns/20 ps	SD |angle|	2

Ab-initio DFT calculations

We computed the frontier orbitals energies at the B3LYP-631g(d,p) level of the aromatic core of a pore in two conformations: a twisted, **TIPS-CMP**, conformation (partial optimization) and a flat, **Aza-CMP**, conformation (full optimization). In addition, the ***twisted*-HATNA** properties calculated at the same level are presented for comparison (Table S3).

Table S3. B3LYP-631g(d,p) calculated electronic properties (all energies are in eV).

	LUMO+2	LUMO+1	LUMO	HOMO	HOMO-1	HOMO-2	gap
TIPS-CMP Twisted aromatic core	-3.66	-3.67	-3.77	-5.82	-5.83	-5.85	2.1
Aza-CMP Flat (D_{6h}) aromatic core	-3.71	-3.71	-3.81	-5.83	-5.83	-5.83	2.0
***twisted*-HATNA**	-2.62	-2.63	-2.98	-5.82	-5.87	-5.87	2.8

Adsorption on graphite

The adsorption of TIPS-CMP on graphite surfaces was studied using the molecular analogue adsorbed on monolayer graphene (Figure S13). In order to allow for the molecule to relax on the surface we performed Molecular Dynamics (MD) simulations at 298 K and 500 K with the molecular mechanics MMFF94 force field using a home version of the software Tinker. Stochastic dynamics with a friction coefficient of 2 ps^{-1} was used to improve conformational sampling. Simulations were run for 1 ns, after which the final conformations were optimized with MMFF94. Standard MMF94 parameters overestimate the intermolecular distances in π-π systems,[6b] to account for this the adsorbed geometries were also optimized using van der Waals MMFF94 parameters "corrected" to reproduce accurately the molecular geometry of the benzene dimer.[6b] The average height of the atoms in the adsorbate molecules with respect to the surface for all models are summarized in table S4.

Table S4. Average heights for the molecular analogue of TIPS-CPM on graphene with different force field parameters.

Standard MMFF94, MD T=298 K	8.04 Å
Standard MMFF94, MD T=500 K	8.11 Å
Corrected MMFF94, MD T=298 K	7.72 Å
Corrected MMFF94, MD T=500 K	7.83 Å

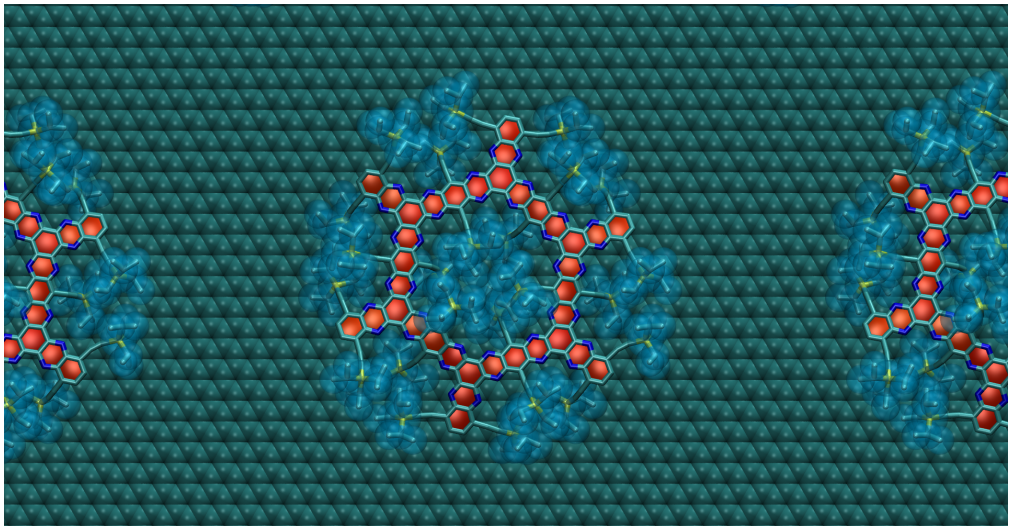

Figure S12. Top view of a TIPS-CPM molecular analogue adsorbed on graphene. Only C (light blue), N (dark blue), and Si (yellow) atoms are rendered. The aromatic rings are emphasized in red, while the C atoms in TIPS groups are rendered as semi-transparent spheres. Structure computed by geometry optimization with corrected MMFF94 parameters from an MD simulation at 298 K.

12. Catalytic activity for the Oxygen Reduction Reaction (ORR)

To evaluate the catalytic ability of **TIPS-CMP** for the Oxygen Reduction Reaction (ORR), a GC electrode was covered by dropcasting with a suspension 0.2 mg/mL in TFA, depositing a total amount of 50 µL (catalyst loading of 140 µg/cm^2). Thus prepapared modified electrodes were used as working electrodes in the ORR experiments in ultrapure KOH 0.1M at a scan rate of 10 mVs^{-1}.

Koutecky-Levich analysis. By representing the limiting current of ORR (at a certain potential) as a function of the rotation speed, the number of electrons involved in the ORR process can be estimated by the slope of the fitting line with Equation S1:

$$n = \frac{1}{0.62\, b\, F A C_0 D^{2/3} v^{-1/6}}$$

Equation S1.

Where F is the Faraday constant (96500 C), C_0 is the oxygen concentration in KOH (8.4x10^{-7} mol/cm^3), A is the electrode surface area (0.07 cm^2), D is the diffusion coefficient (2x10^{-5} cm^2 s^{-1}) and *v* kinematic viscosity (0.008977cm^{2}s^{-1}).[7]

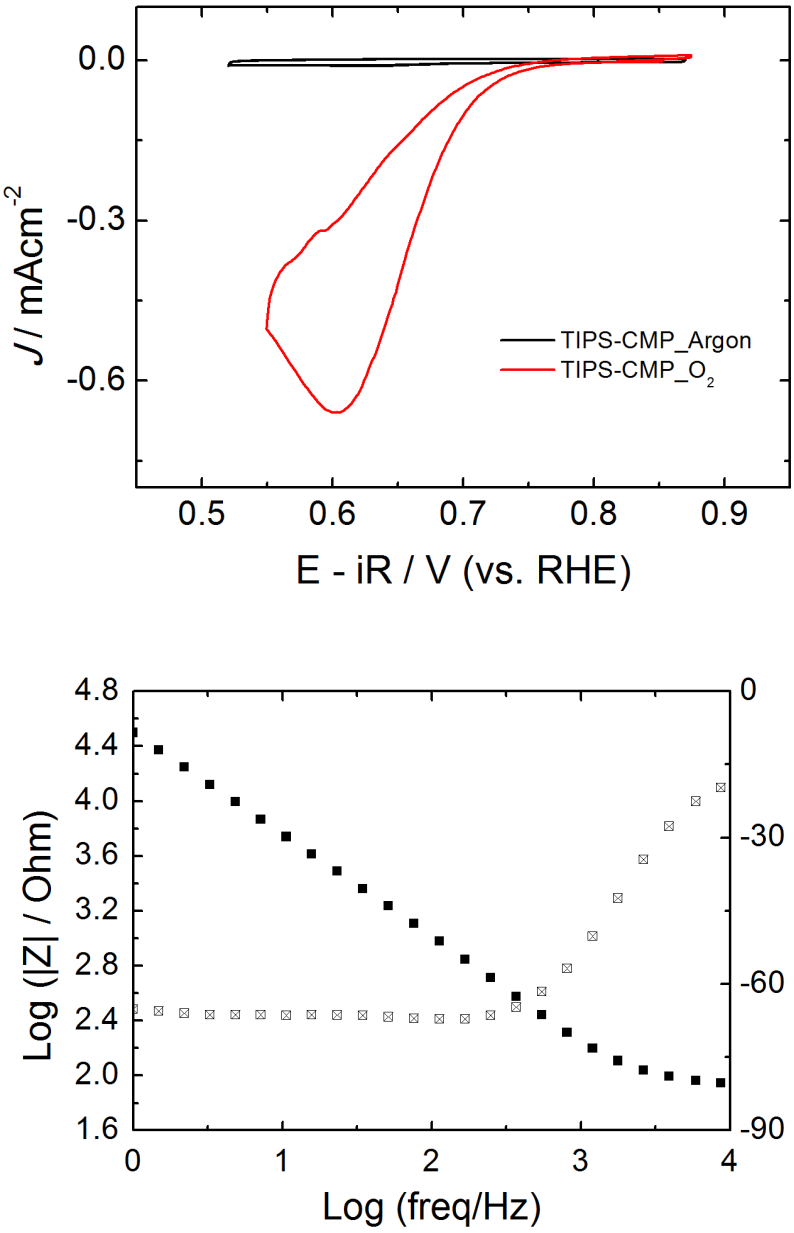

Figure S13. (Top) Representative cyclic voltammogram for **TIPS-CMP** in Ar (black line) and O_2-saturated (red line) KOH 0.1 M. Electrode without rotation. Scan rate: 50 mV/s. (Bottom) Impedance measurements for the determination of solution resistance.

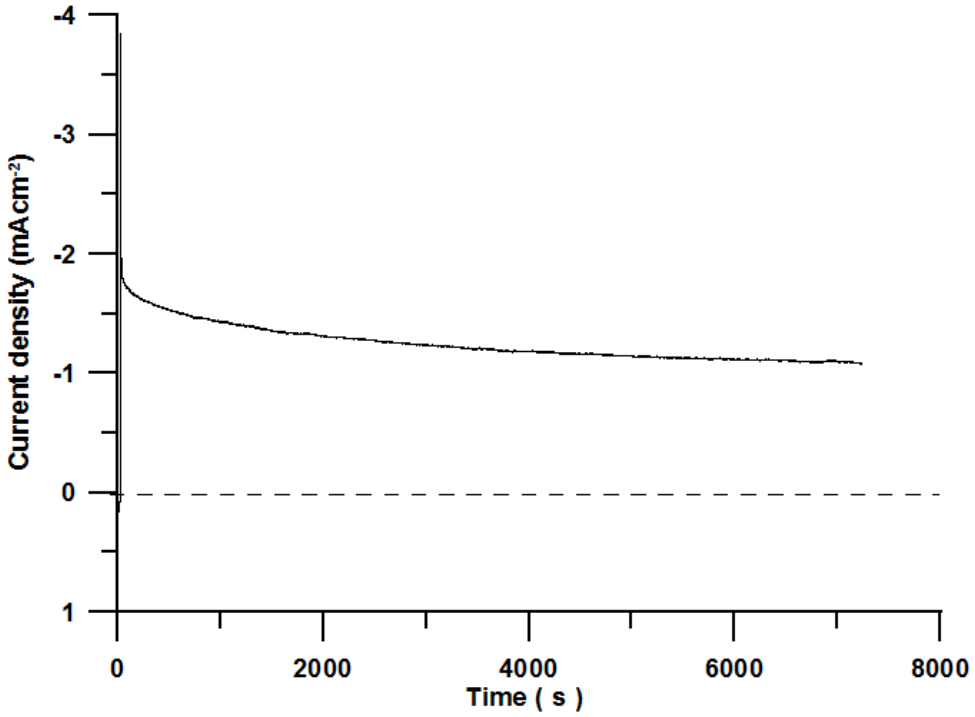

Figure S14. Potentiostatic electrolysis at *E* = 0.6 V_{RHE} for **TIPS-CMP**-casted for O_2-saturated in aqueous ultrapure 0.1 M KOH (rotating speed 1600 rpm).

13. References.

1. A. B. Marco, D. Cortizo-Lacalle, C. Gozalvez, M. Olano, A. Atxabal, X. Sun, M. Melle-Franco, L. E. Hueso, A. Mateo-Alonso, *Chem Commun.,* **2015**, *51*, 10754–10757.
2. a) Côté, A. P.; Benin, A. I.; Ockwig, N. W.; O'Keeffee, M.; Matzger, A. J.; Taghi, O. M. *Science* **2005**, *310*, 1166–1170; b) Spitler, E. L.; Koo, B. T.; Novotney, J. L.; Colson, J. W.; Uribe-Romo, F. J.; Guitierrez, G. D.; Clancy, P.; Dichtel, W. R. *J. Am. Chem. Soc.* **2011**, *133*, 19416–19421.
3. M. D. Hanwell, D. E. Curtis, D. C. Lonie, T. Vandermeersch, E. Zurek, G. R. Hutchison, *J. Cheminform*. **2012**, *4*, 17.
4. J. D. C. Maia, G. A. Urquiza Carvalho, C. P. Mangueira, S. R. Santana, L. A. F. Cabral, G. B. Rocha, *J. Chem. Theory Comput.* **2012**, *8*, 3072–3081.
5. a) M. Korth, M. Pitoňák, J. Řezáč, P. Hobza, *J. Chem. Theory Comput.* **2010**, *6*, 344–352; b) K. Strutyński, J. A. N. F. Gomes, M. Melle-Franco, *J. Phys. Chem. A*, **2014**, *118*, 9561–9567.
6. S. Choudhary, C. Gozalvez, A. Higelin, I. Krossing, M. Melle-Franco, A. Mateo-Alonso, *Chem. Eur. J.*, **2014**, *20*, 1525–1528.
7. Davis, R. E.; Horvath, G. L.; Tobias, C. W. *Electrochim. Acta* **1967**, *12*, 287–297.